Muon Capture on the Deuteron

The MuSun Experiment

PSI Experiment R-08-01, spokespersons P. Kammel, C. Petitjean, A.A. Vasilyev

MuSun Collaboration [1]

Petersburg Nuclear Physics Institute – University of Washington Seattle –
Paul Scherrer Institut – University of Kentucky – Boston University – Regis
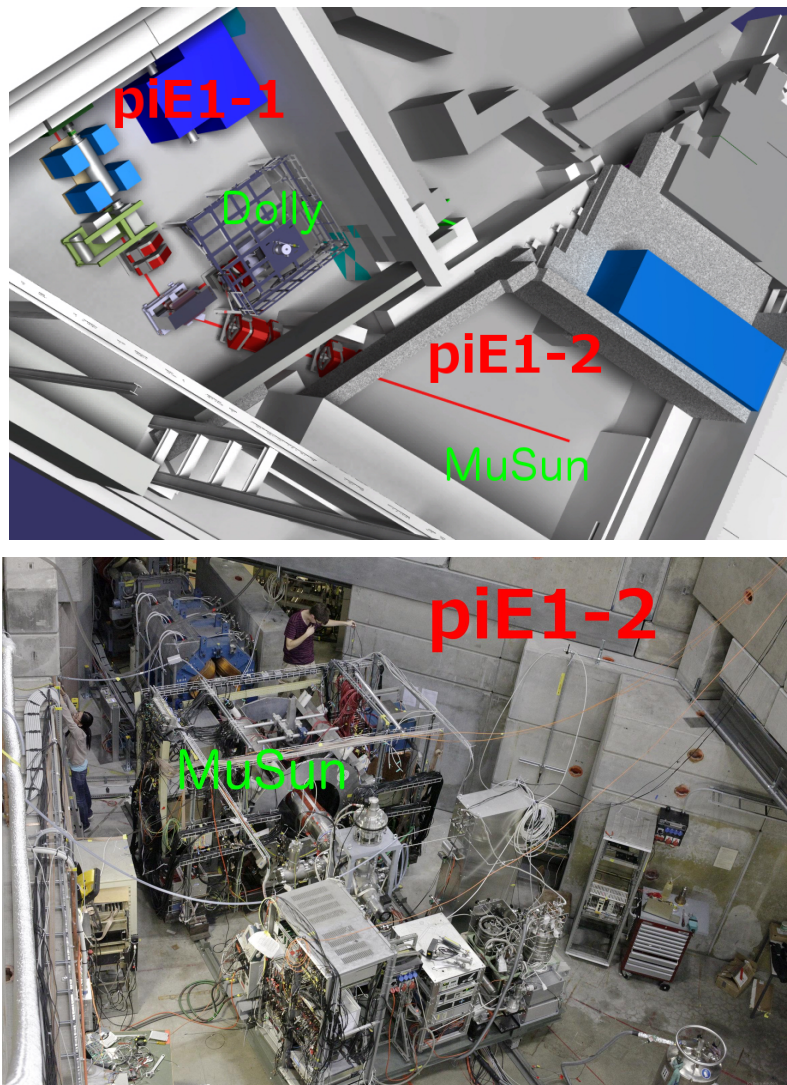University – University of South Carolina– Université Catholique de Louvain

http://muon.npl.washington.edu/exp/MuSun

Figure 1: New πE1 area. Top: CAD layout with μSR Dolly apparatus and extension for MuSun, Bottom: MuSun installed Nov. 2012.

Contents

1 Overview

1.1 Physics Update and Experimental Strategy

We are now at the confluence of two exciting developments in the field of muon capture [2]. Based on the novel "active target" technique developed by our collaboration, experiments on hydrogen and the lightest nuclei are approaching sub-percent precision, surpassing the precision of previous generations of experiments by about an order of magnitude. At the same time, following Weinberg's pioneering approach, effective field theories (EFTs) have been systematically constructed to calculate electro-weak observables in few-body systems. Thus simple nuclear systems become amenable to rigorous QCD-based calculations. On the one hand, these calculations can provide precise results, including a systematic evaluation of their uncertainties. On the other hand, they can establish quantitative relations between muon capture and electro-weak astrophysical processes of fundamental importance, which have never been measured directly. These include pp fusion, which is the primary energy source in the sun and the main sequence stars, and the νd reaction, which provided convincing evidence for solar neutrino oscillations at the Sudbury Neutrino Observatory.

The prime example is the process

$$\mu + d \to n + n + \nu \tag{1}$$

which is the simplest muon capture process on a nucleus. The basic pseudoscalar coupling g_P required for such calculations has been measured by the MuCap experiment.

In modern calculations of the capture rate Λ_d for process (1), the standard nuclear physics approach (SNPA), based on the impulse approximation with explicit modeling of two-body current contributions, is being replaced by less model-dependent hybrid EFT calculations; a pion-less EFT calculation has also been performed. In Fig. 2 theoretical results since 2000 are compared to all existing experimental data. The prospect for a precise MuSun result has stimulated recent calculations, and in 2012 the first full EFT calculations were published [3, 4]. Contrary to the hybrid approach, forces and currents are derived within the same EFT framework. The theoretical program of calculating electro-weak reactions from first principles is not finished yet, see the discussion [3, 4]. In particular, significant effort is expended on consistently treating the three-body forces at the same chiral order (N3LO) as the two-nucleon potentials. The MuSun result will determine the sole unknown low-energy constant (LEC), $\hat{d}_R$ or c_D, involved in an EFT calculation of weak two-nucleon reactions. It will be a benchmark result for extending the EFT method to more complicated few-body processes. Unfortunately, the present experimental situation is unsatisfactory. The best existing experiments [5, 6] are not precise enough and the most precise result differs from modern theory by three standard deviations. If true, such a discrepancy would have major ramifications for the above-mentioned astrophysics processes.

The goal of the MuSun experiment is the measurement of the rate Λ_d to a precision of better than 1.5%. Λ_d denotes the capture rate from the doublet hyperfine state of the muonic deuterium atom in its 1S ground state. This measurement will clarify the current tension between experiment and theory and provide a benchmark commensurate with the expected precision of ongoing, modern calculations. For the foreseeable future, the MuSun experiment is the only theoretically clean way to determine the important axial low-energy constant, which is required for calculating both μd capture as well as pp fusion and νd scattering. The anticipated precision is 5 times greater than presently available from the 2N system and will be essential for calibrating these reactions in a model-independent way.

The MuSun experiment is built on the MuLAN and MuCap techniques developed at PSI. Like MuCap, it is a measurement of the negative muon lifetime in a gaseous tracking
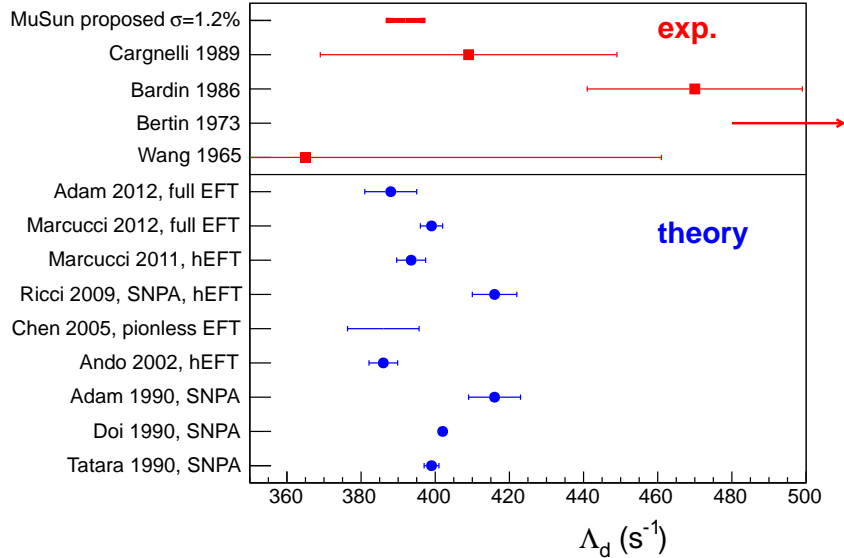
Figure 2: Bottom panel: Recent theoretical results on muon capture rate Λ_d from the doublet state of the μd atom. SNPA denotes potential model calculation, hEFT is hybrid EFT calculation. The pion-less EFT calculation [7] cannot be expressed by a single value and only its intrinsic uncertainty range is indicated. Top panel: Experimental results scatter widely and most accurate result is inconsistent with modern theory.

chamber. The experiment must be performed under conditions such that Λ_d can be extracted unambiguously, independent of muonic atomic physics complications occurring after the muon stops in deuterium. The transition between the upper μd quartet to the lower μd doublet hyperfine state is slow and, once a $dd\mu$ molecule is formed, muon-catalyzed dd fusion occurs within nanoseconds. Our studies demonstrated that atomic physics uncertainties are reduced to a negligible level at optimized target conditions of T = 30 K and 6% liquid hydrogen density. To achieve such conditions, a new high-density cryogenic ionization chamber filled with ultra-pure deuterium has been developed. This Time Projection Chamber (TPC) must define the muon stop, identify impurities, and observe muon-catalyzed reactions. It must have very good energy resolution and full analog readout using flash ADCs. This information is critical to avoid systematic uncertainties in the muon stop definition and to detect the charged particles induced by the fusion and impurity capture processes. Since the target density of MuSun is five times higher than that of MuCap, the chamber does not have internal gas gain and drift voltages up to 80 kV are required.

1.2 Highlights 2012

1.2.1 Commissioning of New piE1 Area

As πE3 became a dedicated high-field μSR area by end of 2011, PSI built a new πE1 area with an extended low-energy muon beamline dedicated to particle physics experiments (see Fig. 1). The first part πE1-1 of the beamline serves as a permanent space for the Dolly μSR facility. The extension πE1-2 became the new fixed location for the MuSun experiment. It can be separated from the upstream area by a wall. The complex MuSun apparatus does not have to be craned out after each run, saving weeks of work, and can be tested and optimized during

μSR beamtime. The area became ready in September 2012, the beamline was tuned by part of the MuSun collaboration in late September, and the complete experiment was installed into the area in October 2012. All systems became operational during a 4 week commissioning period and first data in the new area was successfully taken. The verification of the beam quality for negative muons, extracted and measured carefully for the first time with the new beam optics, was a critical milestone for the experiment, and, fortunately, excellent conditions could be established. The MuSun collaboration would like to express its gratitude to the PSI management and staff, who achieved this major installation effort within a tight schedule.

1.2.2 Analysis of Production Run 2011

During the last run in the previously used πE3 area in 2011, a first production run with significant statistics was achieved. This motivated a focused effort to move forward with the data analysis according to our Analysis Roadmap. We expect a first physics result from this data. At the same time we have and are upgrading the experiment in several respects, to aim for full production in 2013 and 2014 with significantly reduced statistical and systematic uncertainties compared to the initial 2011 run. Further corroboration that several challenges faced by MuSun are under control comes from the final, highly consistent analysis of the MuCap experiment, whose results were released in 2012 and just accepted for publication in PRL [8].

2 Commissioning Run R2012

2.1 Commissioning of New Low Energy Muon Beam

2.1.1 The new muon beamline and πE1-2 area

Since the πE3 beam which was previously used by MuSun is no longer available for particle physics, a new low-energy muon beamline was constructed in the existing πE1 area with extension into the former NE-B low energy area - now called the πE1-2 area. Fig. 3 shows a CAD design drawing of the new low energy muon beamline. The wall between these areas has been replaced by a bridge allowing the muon beam to go underneath into πE1-2 after a 38° bend in magnet ASK51. The new area provides sufficient space for setting up the MuSun experiment with all supplies. The apparatus can be rolled back and a shielding wall can be placed after the bridge. In this case the πE1-2 area can be used for servicing and commissioning the MuSun experiment while the original πE1-1 area can use the beam, e.g. for the DOLLY μSR facility. The only beamline elements that need to be removed are the kicker and separator which are exchanged for the spin rotator. In 2012, two provisionary quadrupole triplets were set up for MuSun, since the final magnets are still on order. The second triplet had only an 18 cm instead of a 30 cm aperture, which caused a significant reduction of the available beam phase space for 2012.

Fig. 4 displays the calculated beam envelopes after optimization with the TRANSPORT code. Turtle calculations have confirmed excellent beam quality concerning the beam spot and resolution. The solid angle accepted from the proton target is 15 msr. The ideas behind this beam design are as follows:

- High beam quality (small phase space, dispersion-free) and high momentum resolution ($\pm$0.5-3.0%, variable) of the existing πE1 beamline in the main shielding wall (original design by R. Frosch).
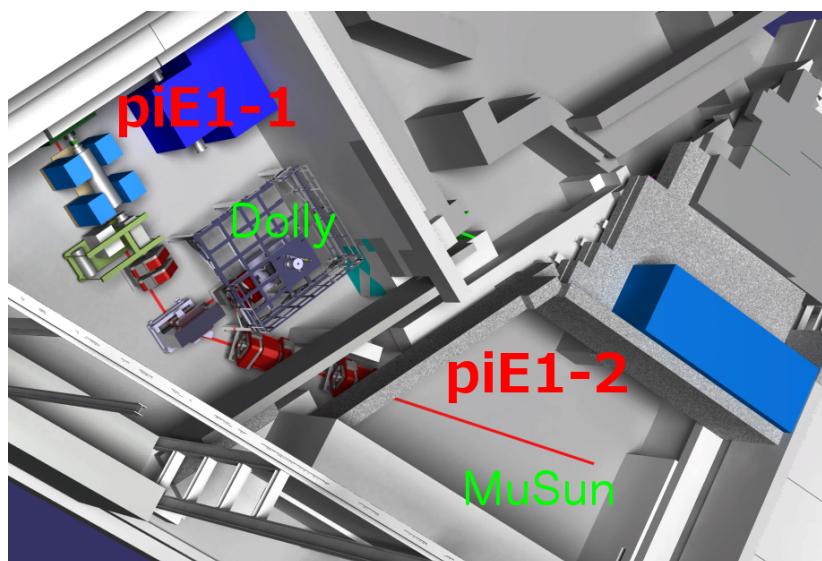
Figure 3: CAD drawing of the new πE1 low energy muon beam. The visible beam elements are (in order from the proton channel) are: kicker - electrostatic separator - quad doublet QSE51/52 - bending magnet ASK51 - quad triplet - slit system FS54 - quad triplet. The electronics barrack is located just above the new πE1-2 area. The element in the top corner is the spin rotator which is used when DOLLY runs. ASK51 turns then the beam 90° to the left.

- (Vertical) MuLAN kicker to get pileup-free muons ("muon on request" mode) which yields three times as many pile-up free muons compared to conventional electronic pileup protection.

- (Vertical) electrostatic separator to clean off the intense electron contamination originating from π^o production in the proton target. At forward production angles, the electron background is very intense and must be efficiently eliminated.

- Muons bent with magnet ASK51 towards the πE1-2 area to obtain enough length for cleaning and refocusing the beam. The muon beam is double focused in the center of ASK51 which allows (horizontally) to keep it non-dispersive and (vertically) to cut off the deflected electrons and the kicked muons by using a collimator.

- First quadrupole triplet to refocus the beam from ASK51 onto a slit system. This allows to clean off efficiently any remaining tails from electrons and muons. With the slits, one can also adjust the final beam spot at the experiment.

- Second quadrupole triplet to refocus the clean muon beam onto the experimental target.

2.1.2   First beam studies at the πE1-2 beam window

The first tests with the full muon beamline were performed late September in a shielded cave using plastic scintillation counters placed right after the vacuum window, 80 cm from the last triplet. One detector, 14x14 cm^2, d = 5 mm, was set up to determine and optimize the total flux of the beam, and a second detector, a small scintillator pill (diameter and thickness 2 mm each) was mounted on a scanner device to study and optimize the beam profiles. Both detectors had good discrimination between electrons and muons.
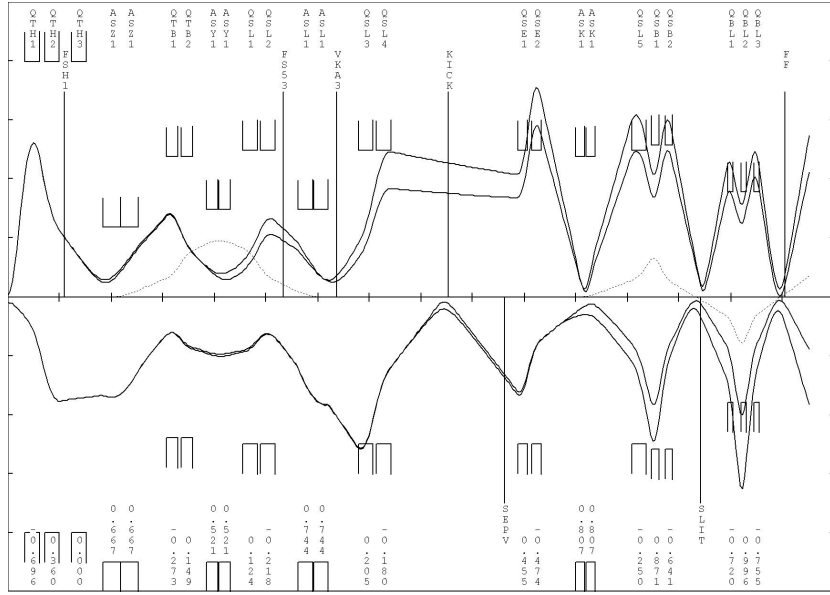
Figure 4: Transport output of optimized beam envelopes of the 2012 πE1 muon beam calculated in first and second order. The upper half gives the vertical envelope, the lower half gives the horizontal. The 1% beam dispersion is indicated by the dotted line showing that $\pm 1\%$ momentum resolution can be obtained by setting the slits in the second magnet to ± 5 cm. In the entrance part of the πE1-1 area the beam is made vertically wide and parallel which gives for the kicker and separator the maximum separation effect. Vertical scale ± 25 cm, beam length up to final focus is 30 m.
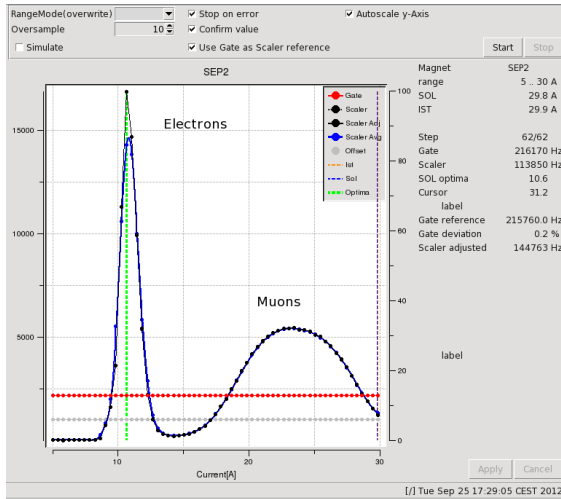
Figure 5: Scan of the separator magnet current, taken with the 28 MeV/c surface μ^+ beam. As the current is increased, first the electrons appear, then the muons. A magnet current is then chosen to optimize the muon rate.

Figure 6: A 2 mm thick, 2 mm diameter scintillator on a small PMT was used in many of the beam commissioning tests conducted in R2012. This figure shows it at the zero degree exit of bending magnet ASK51. Beam positrons and muon decay positrons are detected.

7

Figure 7: The electron and muon rate at varying vertical positions, measured using the pill detector at the zero degree exit of ASK51. The green (muons in Hz) and purple (electrons in kHz) data points give the rate with the separator off. With the se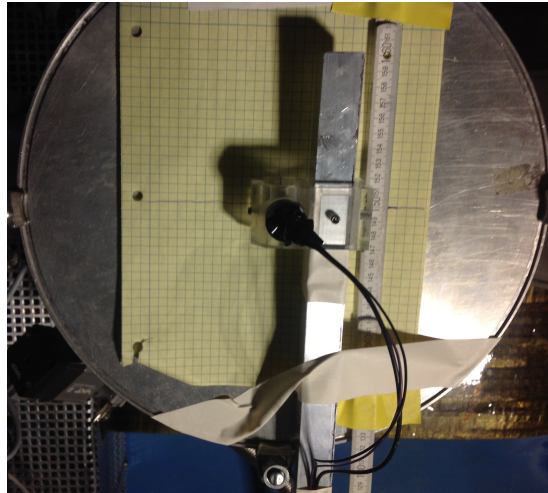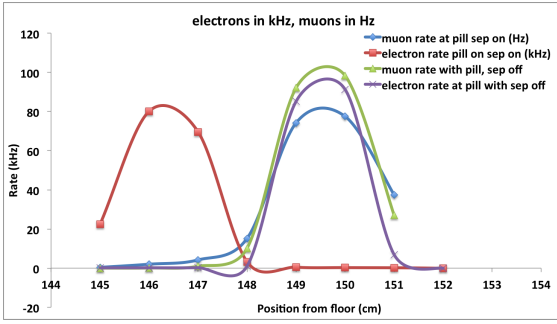parator on, the electrons shown in red are shifted down by ~ 3.5 cm, while the position of the muon beam (in blue) remains unaffected.

Figure 8: Photo of the brass collimator placed in the center of the bending magnet ASK51. The electrons that are deflected by the electrostatic separator stop in the brass.

The tunings and optimizations were done with the help of EPICS, the new PSI-designed set point system, combined with a redesigned OPTIMA software. An example of such a scan is given in Fig. 5.

First the 28 MeV/c surface μ^+ beam was tuned and the electrostatic separator tested (Fig. 5). Since our detectors were rate limited to 1-2 MHz, we worked with narrowed momentum slits, but interpolated to open slits, the highest observed 28 MeV/c μ^+ rate reached 5.4 MHz in nice agreement with the observations made in the September 2010 πE1 beam test. At 42 MeV/c, with momentum slits ± 2.5 cm, 162 kHz μ^+ and 62 kHz μ^- were recorded, again in good agreement with the 2010 data.

The observed positron (electron) contaminations in the muon beam were found initially to be 253 kHz (e^+) and 100 kHz (e^-) respectively, giving an unsatisfactory e:μ ratio of 1.6. A solution to this problem was found by studying the beam in the zero degree prolongation behind the ASK bending magnet. The set up is shown in Fig. 6. The most important result of the scans at this position is plotted in Fig. 7 and demonstrates efficient separation of electrons from muons by about 3.5 cm at 42 MeV/c (separator high voltage at 190 kV).

Finally, the pill detector was placed right in the center of ASK51. This allowed us to tune the beam right at the place where a double focus is required. The most effective removal of the electrons was finally achieved by placing a vertical brass collimator of 20 mm aperture, 30 mm thickness in the center of ASK51, see photo Fig. 8. The chosen size of the collimator was improvised based on transport calculations. For future operations it will be indispensable to have a remotely adjustable collimator installed. With this arrangement we achieved a ratio $R(e/\mu^-) = 0.7$ at 42 MeV/c which is acceptable, but can certainly be improved in the future. The success of the beam optimization is also shown by the excellent beam profiles which were finally obtained resulting in FWHM widths of only 11 mm (horizontal) and 9 mm (vertical), respectively. These profiles are presented in Figs. 9 (42 MeV/c μ^+ beam).

2.1.3   Tests and measurements with the MuSun apparatus

After the apparatus was installed in the new area, beam tests were also performed using the MuSun detectors. The entrance detectors are mounted on the last section of the beamline.
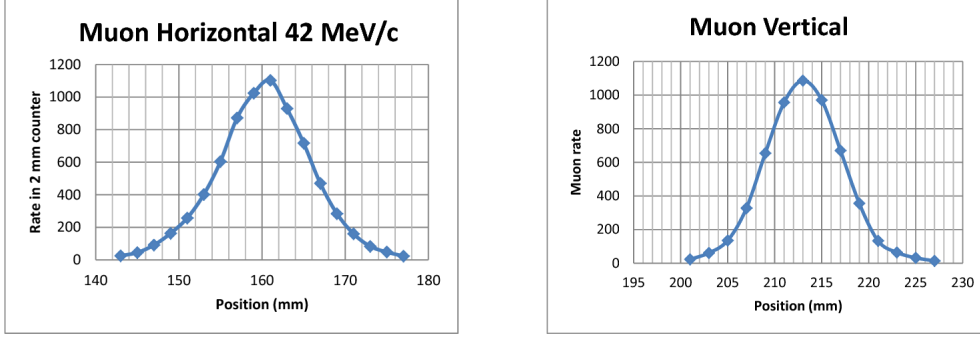
Figure 9: Horizontal and vertical profiles of 42 MeV/c μ^+ beam at the channel end.

This "Beam snout" consists of the main muon-trigger scintillation counter, μSC[1], the veto counter, μSCA, with a 45 mm hole in the center, and a multi-wire proportional chamber, μPC, which provides horizontal (X) and vertical (Y) positions of beam particles.

Figure 10 shows the X and Y distribution of the beam (16 mm × 22 mm FWHM) as measured by the μPC entrance detector. Once the TPC was operational the beam was further tuned to optimize the muon stop efficiency in the TPC. Fig. 11 demonstrates that this efficiency was high ($\geq 60\%$) over the whole beam spot.

The excellent momentum resolution of the πE1 beam is reflected in the muon stopping distribution in the TPC (Fig. 12), where, for the narrow momentum cut, the width of the distribution is dominated by muon straggling in the entrance windows and detectors. However, there is a significant loss of beam rate for a narrow momentum slice (Fig. 13).

The results of the 2012 measurements with the MuSun apparatus have been summarized in Table 1. For future runs, there is still room for improvement with the foreseen large aperture last quad and an adjustable slit system in ASK51.

μSC muon rate with kicker (kHz)	μSC electron rate (kHz)	Stopping fraction in the TPC	Kicker extinction	Beam momentum for $\phi = 0.057$(MeV/c)
23.3	3.5	48.0 %	50-150	37.9 (dp/p=3%)

Table 1: Status of the beam in πE1-1 at the end of R2012. The kicker extinction factor and the muon stop efficiency could not be optimized at the same time, as they both depend on the vertical steering, i.e. separator current.

2.2 Commission of Experiment in New Area

2.2.1 Overall layout

As seen in Fig. 1 the main components of the MuSun experiment are arranged on three platforms, the electron detector platform, the TPC platform, and the gas system platform. The length of the area πE1-2 is 12 m from the last quadrupoles to the back wall. As the three platforms are connected with electrical and vacuum interfaces, they have to be moved simultaneously, while still allowing the flexibility to move the TPC between its service and measurement positions. To allow for all this, the electron and gas platforms are mounted on 10 m long main rails, while the TPC platform has its own precision rail system.

---

[1]A *high* and *low* threshold were set to discriminate muons from electrons.
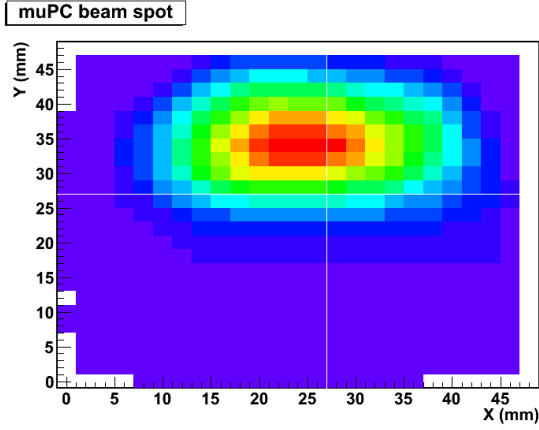
Figure 10: The x and y coordinates of the beam spot (16 mm × 22 mm FWHM) as measured by the μPC entrance detector. The white cross is the the virtual beam axis.
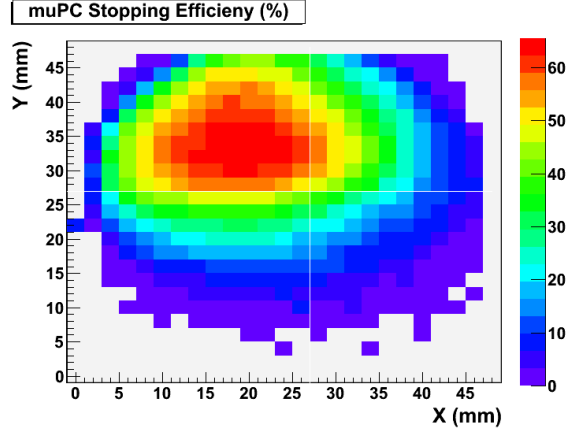
Figure 11: Correlation between the μPC and the muon stop efficiency in the TPC, to which the muon beam was tuned.
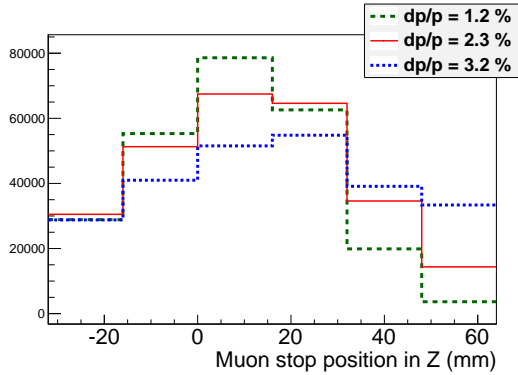

Figure 12: The muon stop distribution in Z for different momentum width. The center of the TPC is at 0 mm.
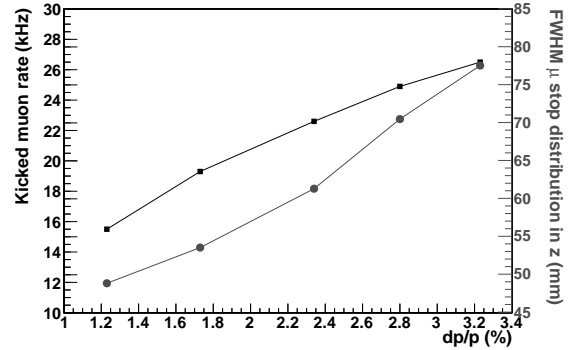
Figure 13: The width of the muon stop distribution in Z ● and the kicked μ rate ■ (38.3 MeV/c) for different momentum widths. The raw incident muon rates go from 24 kHz to 65 kHz.

The overall layout aimed to provide a permanent installation of the MuSun apparatus, while allowing for a significant travel distance of the experiment towards the back wall of the area, freeing up space for a shielding wall towards πE1-1 or for other low muon experiments in the πE2-2 area.

New cable bundles had to be installed, because the signal distance the cable runs are longer than in πE3, and additional length was required to maintain the flexibility to move the detector, while minimizing the interfaces needed to be disconnected. This was achieved by two main cable runs, one in a flexible cable carrier system, which follows the detector and a fixed one to service the beam instrumentation.

Because of the length of the cable runs and the associated signal loss and interference issues, several readout systems were reconfigured so that all analog decision and digitization occurs in the detector area. This digital information is then send to the electronic barrack. The electronic barrack and a new MuSun analysis barrack were installed above the area and were fully commissioned.

In the future, an air conditioned environment has to be build around the experiment. This is foreseen for Spring 2013. The new area does not have the necessary LN2 supply lines, which led to difficulties during weekends, with limited crane operation. A new improved supply system is being designed by PSI staff and PNPI experts.

2.2.2 Alarm system

At center of the MuSun alarm system is a relay box that connects to various sensors throughout the system (Table 2). During R2012, the box was fully rewired, making sure that each alarm had its dedicated relay. The TPC high voltage supply was interlocked with the TPC alarms, where all alarms can trigger a single MIDAS (DAQ) alarm message, at the same time notifying the off-shift crew by telephone. Despite the fact that the interlock functionality was working properly and all gas alarms had a dedicated horn and siren, it became clear that we need a central status panel as a quick diagnostic tool for people on shift. Such a system will be ready for the next running period, together with an interface for remote monitoring.

Alarm	MIDAS interface	TPC HV interlock	Description/trigger
TPC vacuum	✓	✓	Insulation vacuum pressure
TPC pressure	✓	✓	Overpressure in the TPC
Compressor	✓	✓	Status of the compressor for the cold-head
Water pump	✓		Status of the compressor cooling water circuit
CHUPS	✓		General alarm of the CHUPS system
Flammable gas alarm	✓		Gas sensor at bottle and mixer
Kimessa gas alarm	✓		Sensor for D_2 and O_2 levels

Table 2: MuSun alarm/interlock system.

2.3 Upgrades to the MuSun Experiment

2.3.1 Circulating Hydrogen Ultra-high Purification System (CHUPS)

CHUPS cleans and stabilizes the pressure of the D_2 gas for the MuSun TPC. After many years of operation since 2003, several components needed to be replaced. Prior to the R2012 commissioning run, the CHUPS system was substantially upgraded.

The gas system from and to the cryogenic compressor (Fig. 14) was reassembled and optimized, exchanging about 30 valves and fittings and 20 meters of tubes. Both the activated carbon in the compressor and the zeolite in the purifiers were exchanged. New electro-pneumatic valves were installed on the liquid nitrogen filling system. For the next running period, an inconvenient dewar based system will be replaced by a fixed liquid nitrogen supply system.

In addition, the CHUPS control system was modernized, adapting the configuration of the alarm system to the specific safety requirements of the MuSun experiment. Additional check valves were added, including a check valve with a large cross section for the release of pressurized D_2 gas from the vacuum volume in case of emergency, leading the gas outside of the beam area in a controlled manner.
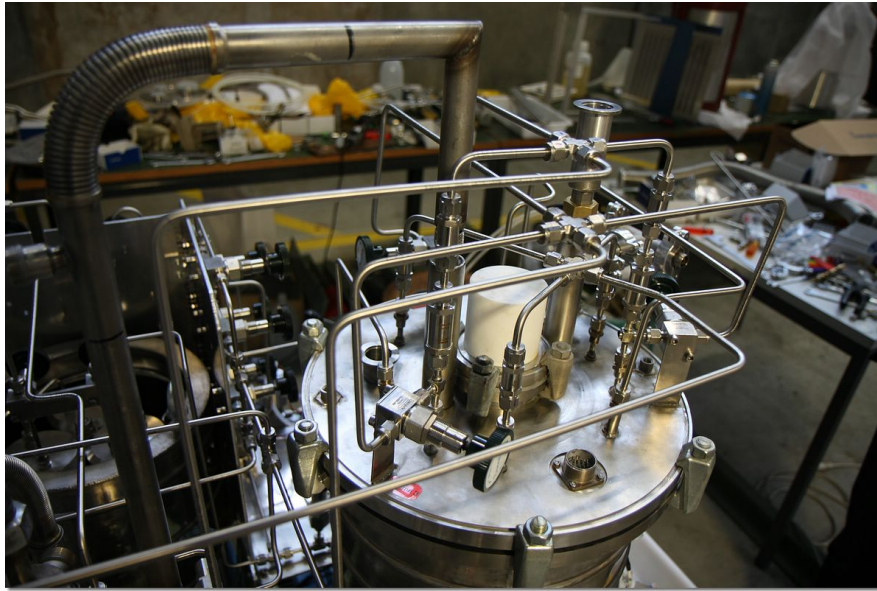
Figure 14: The new compressor gas piping.

2.3.2 Cryo-preamplifiers

The limited energy resolution of $\sim$40 keV (1σ) in R2011 was not well understood[2], and has thus led to a significant amplifier development project. The muon stop definition (e.g. Sect. 3.2.3) and the detection of gas impurities (e.g. Fig. 26) would both benefit from improved energy resolution.

We intend to place a new charge-integrating preamplifier system just outside the TPC, within the insulating vacuum. This location reduces the length of interconnecting cable, and it allows the preamplifier to remain in a fully shielded volume. A short cable can itself be shielded without introducing excessive capacitance, thereby reducing microphonic pickup the cathode high voltage. Finally, this location allows the amplifier to be cooled to cryogenic temperatures to reduce thermal noise.

Low power consumption and an ability to operate over a wide range of temperatures were essential design requirements for the new preamplifier circuit. The TI OPA2211 dual operational amplifier was selected for its low noise and low power consumption. Its silicon-germanium heterojunction transistor structure would be expected to work at very low temperatures, and we have tested it successfully down to 65 K. We have explored several potential front-end transistors, including both traditional silicon JFETs and low-noise dual-gate MOS-FETs. To this point, as shown in Fig. 15, the BF862 silicon JFET has provided the best performance with a test pulser in the laboratory, reaching a resolution of 4.5 keV at an optimal temperature of -150° C (123 K). The circuit consumes only 50 mW per channel at that temperature, compared with 90 mW per channel at room temperature.

To further characterize the different noise contributions to the total electronic chain, power spectral density (PSD) curves as shown in Fig. 16 were measured and analyzed. It was found that the input protection diodes were a major source of parallel Johnson noise, which could be reduced dramatically by cooling them below -100° C. The PSD served as an input to determine the optimum filter and shaping times. Further, the noise slope at room temperature and 0.25 μs shaping times was determined to be 0.26 keV/pF, which still allows the use of a

---

[2]The theoretical limit for a 1 MeV signal is 7 keV, supposing no recombination effects and a 150 electron RMS charge integrating preamplifier.
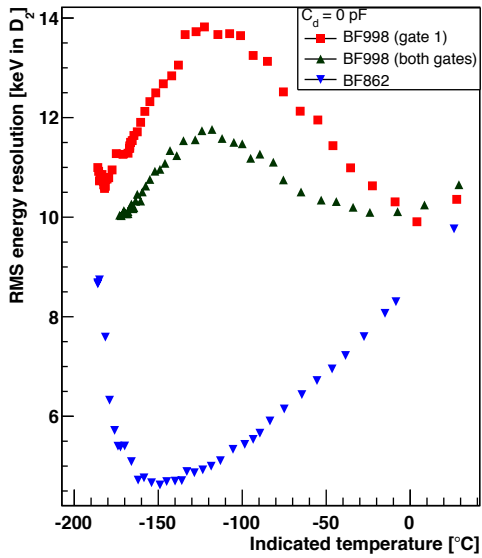
Figure 15: Performance of a cryogenic preamplifier prototype for two front-end transistors: a BF998 dual-gate MOS-FET in two different circuit configurations, and a BF862 silicon JFET. No external input protection circuit was connected.
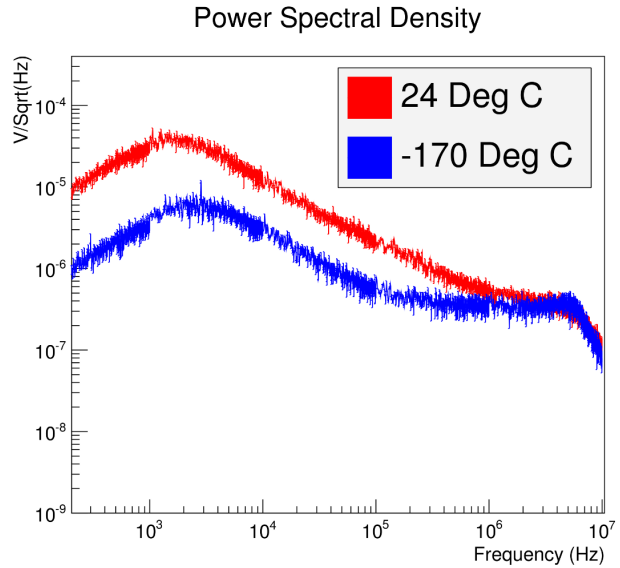
Figure 16: Power spectral density at two temperatures for a preamplifier with a BF862 transistor and input protection diodes. Cooling dramatically reduces the thermal noise. The corresponding energy resolution of the two measurement shown above is 14 keV and 7 keV (1σ).
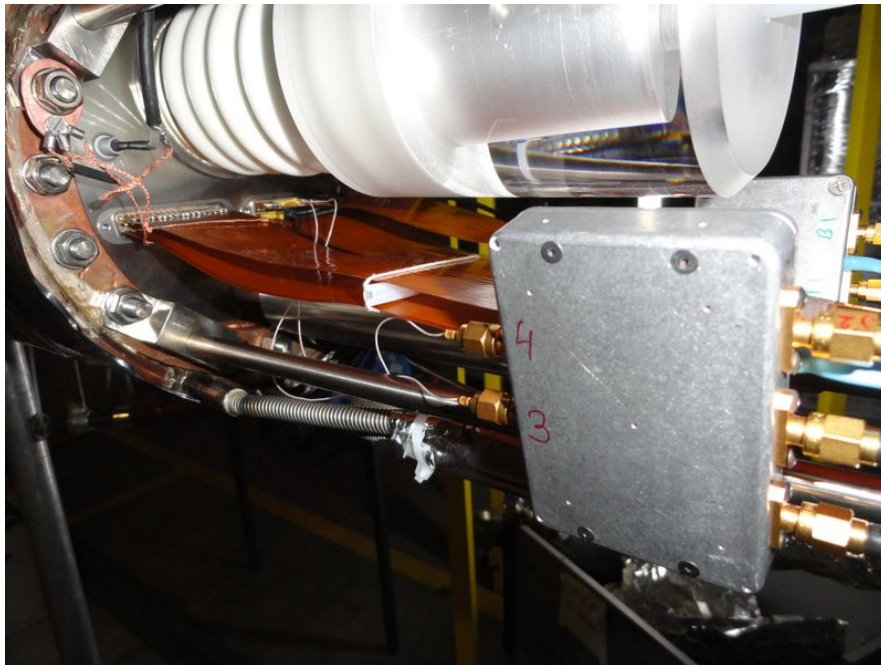
Figure 17: Installation of new preamplifier modules on TPC support rods, see text.

short coaxial cables for the input signal.

Four prototypes with different configurations were installed and operated successfully at PSI. Two modules, each containing two new preamplifier channels were mounted on the TPC support rods 25 cm from the TPC flange, as shown in Fig. 17. For one module, the

preamplifiers were connected to the TPC pad plane via coaxial cables, which proved to be the better choice. The power supply and signal output wires of all preamps consisted of shielded cables running along the TPC support rods and connecting to a flange feedthrough. From the feedthrough the signal wires were then sent to four Ortec shaping amplifiers (0.25 μs shaping time). Once the TPC was cooled to a temperature of 34 K, the temperature of the new preamplifiers was measured to be 260 K. Although the thermal contact with the support rods did not provide the cooling power needed to demonstrate the resolution obtained in the laboratory, an significant improvement in the electronic resolution was achieved (Fig. 18). This is reflected in the energy resolution of physical signals from the TPC (Fig. 19).
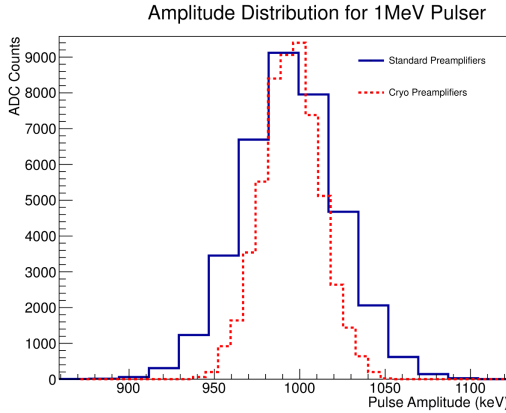

Figure 18: Pulse amplitude distribution of a test charge injected into a standard and a cryo preamplifier connected to the fully operational TPC. The electronics resolution (1σ) is 29 keV and 17 keV, respectively.
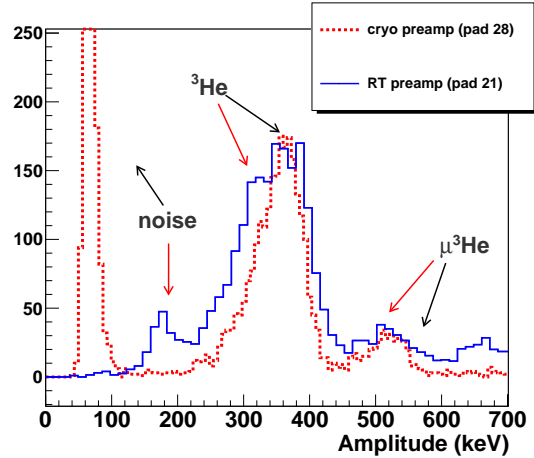
Figure 19: The delayed energy spectrum in the TPC (3 μs $\rightarrow$ 5 μs after the muon stop). The cryo preamplifier shows a large improvement ($40 \rightarrow 25$ keV) of the energy resolution on the ^{3}He fusion peak, with a significant reduction of the background for possible capture recoil signals (see Fig. 26). The noise slope is cut off by threshold at different places for the two curves.

2.3.3 TPC pad plane

The TPC anode pads have to be plated with 40 μm gold or silver surfaces, so that muons would be quickly captured by the high-Z stop material. Our original pads were based on metal coated Macor, which, though machinable, does not provide good peeling strength. After several iterations, we found a supplier who produces thick film metalization based on a Moly-Manganese first layer process. This method is applied to alumina fired at 1400° C and provides high bond strengths. This allows the machining of the pad structure after metalization without peeling of edges. While there was concern about the flatness tolerances in their high temperature process, a first prototype showed good properties and was used during R2012. The final pad plane is currently being produced. The R2012 prototype had a thin metal primer layer coated with a 35-40 μm thick silver layer.

2.3.4 New X-ray detectors

The gas purity requirement of the MuSun experiment is at the parts-per-billion level [9]. Complementary to gas chromatography, an in-situ measurement of these impurities is therefore essential.

The nuclear recoils of muon captures on gas impurities, mainly nitrogen and oxygen at low temperatures, yield localized signals of a few 100 keV in the TPC. Contrary to the MuCap experiment [8], these signals are not background free, with a large background from ^{3}He muon-catalyzed fusion events. Capture signals were found in the R2011 data (Fig. 26), but it remains a challenge to make a quantitative measurement of the capture yield at nominal conditions[3].

As a first step, the TPC energy resolution needs to be improved. Critical progress was made with our preamplifier upgrades (see Sect. 2.3.2). Secondly, an additional tag with a muonic X-ray, which are emitted with a near 100 % probability when a muon transfers from a μd to a μZ atom, is a promising tool to further clean up the ^{3}He background. The challenges for this method are:

- **Detection efficiency:** A sufficiently large solid angle is needed. For 10^9 muon stops in the TPC and 1 ppb of N_2, a detection efficiency of a 3% is needed to tag > 100 capture signals.

- **Background:** In the few μs time window between the muon stop and the candidate capture signal, the background rate has to be lower than the detection efficiency. A good energy resolution is required.

The solid angle requirement rules out the use of germanium detectors. To keep the background low, we still need a decent energy resolution, which limits us to NaI(Tl) or CsI(Tl). During the 2011 run, a first test was performed with standard 3"x3" NaI detector, which had an energy resolution of 15 keV FWHM at 122 keV, and a background rate of 100 Hz with an efficiency of 0.1 % in the regions of interest[4], yielding a signal to noise of 3/1. For R2012, two new X-ray detectors were constructed, consisting of a 10 cm $\times$ 1 cm NaI(Tl) and a 10 cm $\times$ 1.5 cm CsI(Tl) disc-shaped crystals coupled to 5" PMT tubes. They were mounted facing the TPC vessel, each having a detection efficiency of 0.7 % at 100 keV.
It is a challenge to maintain good energy resolution with larger sized crystals and large PMT's. The NaI prototype had an reasonable energy resolution of 22 keV FWHM at 122 keV. However, the CsI prototype resolution was rather poor, 37 keV at 122 keV, with a non-gaussian full energy peak, suggesting a non uniform detector response. In the coming year, the detectors will be further optimized by improving the light collection efficiency, the addition of a light guide/mixer, and quantification of the non-uniformity of the quantum efficiency of the photocathodes. If in addition, the background rate of these detectors proves to be sufficiently low (with analysis cuts), we will build an array of 5 X-ray detectors which will be deployed for a dedicated impurity concentration measurement.

3 Analysis R2011

3.1 Analysis Overview

Analysis of R2011 data has realized working software toolsets, high-level physics studies, and an established MuSun simulation framework. The R2011 Analysis Roadmap (Fig. 20) shows

---

[3]The capture yield for N (O) is 2.7 10^{-6} (1.6 10^{-6}) per ppb.
[4]The 2p→1s X-ray is 103 keV and 135 keV for N and O, respectively.

the progress in the past year. Green check marks indicate tasks that have been completed or that are well understood. Orange arrows indicate high priority analysis tasks or studies that will inform present data acquisition developments. Most of the low-level tasks under "Documentation and Quality Control," "Software Framework and Development," and "Basic Analysis," as well as a few high-level studies have been completed.

While the focus of work in the last half of 2011 was the renovation of software tools, 2012 has seen these tools become standardized and robust. Systematic sectioning and categorization of the R2011 dataset facilitates simple quality and data consistency checks and provides a framework for further division of the data should it be required. The Stage 1 analysis code has achieved robust standardization, allowing a full pass of the R2011 dataset to be completed. The Stage 2 analysis code is now used for rapid passes over the Stage 1 output, performing additional calculations and producing decay time distribution histograms. A package of decay time distribution fitting routines has been created to standardize the fitting algorithm, display the variation of fitted lifetime with analysis cuts, and implement additional blinding measures.
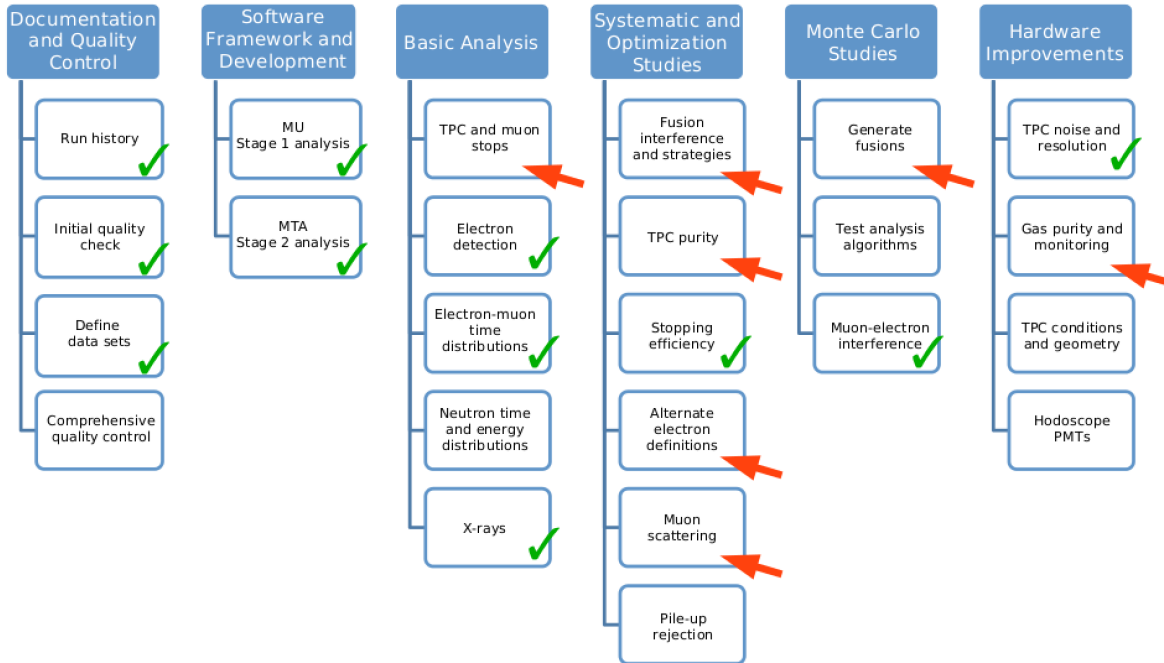
Figure 20: Outline of MuSun Analysis Plan, see text.

Additional refinement of the neutron definition yielded improvements in the pulse shape discrimination and treatment of pulses larger than the ADC dynamic range. An upgrade to the electron tracking definition that treats information from all detectors equally is nearly completed and will be deployed in the next full pass of the Stage 1 analysis.

The MuSun Monte Carlo simulation software has undergone development to incorporate all detector systems, the electronics response of detectors, and the full muon atomic kinetics. This GEANT4 model has been used for several studies related to known systematic effects in lifetime measurements. In particular, the effect of electron interference with the TPC muon stop definition (well-known from MuCap) has been quantified, and an alternate stopping definition based on upstream pads has been tested. Finally, a combination of beam data with auxiliary X-ray detectors and Monte Carlo simulation has illuminated the source of beam muon losses. This sheds light on the surprising observation that only 60% of muons seen in the entrance counters make any signal in the TPC.

Data set	# Runs	μSR Magnet	PMT Shielding	ePC2 HV
prod_rn4_mu+_a	1524	✓	✓	2850
prod_rn4_mu-_a	429			2800
prod_rn4_mu-_b	119	✓		2850
prod_rn4_mu-_c	139	✓		2800
prod_rn4_mu-_d	2072	✓		2800
prod_rn4_mu-_e	71	✓	✓	2830
prod_rn4_mu-_f	1986	✓	✓	2800
prod_rn4_mu-_g	3760	✓	✓	2850
prod_rn4_mu-_h	1365	✓	✓	2850
prod_rn4_mu-_i	3293	✓	✓	2800

Table 3: MuSun R2011 production data sets. One run corresponds to 4 minutes of data acquisition, or 2×10^6 pile-up protected muons.

Data set	# Runs	Comment
clocked_kicker	24	Pile-up detection efficiency study
cosmics	256	Beam off, but all detectors active
density_scan	294	Changing D_2 gas density
no_kicker	59	Production data without the kicker
tscan1	560	Changing D_2 gas temperature, first time
tscan2	961	Changing D_2 gas temperature, second time

Table 4: MuSun R2011 special data sets for systematic studies.

The analysis of R2011 data has undergone considerable development where physical information is more readily extracted and compared to expectations from simulation and calculation. With established algorithms for detector sub-systems, the analysis is at the level of measuring systematic lifetime shifts due to analysis cuts and on track to extract a result for Λ_d from the R2011 data.

3.1.1 Data Sets and Analysis Software

R2011 Datasets and Quality checks The data collected in R2011 is divided into groups of runs with similar experimental conditions. Classification is based on conditions that are known to have varied, including the bias voltage on wire chambers, the magnetic shielding of neutron detector PMTs, and the amplitude of the muon spin rotating magnetic field. The datasets are summarized in Tables 3 and 4. This organization will be adapted as further meaningful differentiation of the data becomes necessary.

Stage 1 Analysis: *MU* Analysis of MuSun data is performed with a multi-stage approach. Stage 1 analysis uses the *MU* framework, which performs initial quality checks and collects data from multiple channels into physics objects, such as electron tracks. In particular, clustering in the wire chambers and pulse-fitting for TPC signals is performed at *MU*-level. Processing the entire production dataset from R2011 requires between 10000 and 20000 cpu-hours, depending on the computing hardware used. A first pass of *MU*-level analysis on the full R2011 production dataset was performed in June 2012 at the TACC supercomputer Lonestar. Analysis of runs dedicated to systematic studies, such as runs at different D_2 densities and temperatures, is performed at a smaller scale on local machines or university

clusters. The MuSun collaboration maintains an allocation of 200,000 SU (cpu-hours) per year at the Lonestar cluster.

Stage 2 Analysis: *MTA* With data organized into physics objects, the Stage 2 analysis forms correlations between detector systems with the ultimate goal of measuring the average lifetime of muons that have stopped in pure D_2 gas. The ongoing analysis is at the level of measuring shifts in the fitted lifetime due to varying the parameters of the electron track definition, the muon track definition, and other observables. For example, a variation of the lifetime with stop position in the TPC is an indication that the stop definition is accepting muons that are not really in the D_2 gas, or that the tracking cut rejects muons in a time-dependent manner. All such variations must be understood and eliminated or corrected to confidently extract the capture rate, Λ_d. The Stage 2 analysis, *MTA* is primarily a routine to loop over the events from the Stage 1 analysis, producing histograms. Processing the full R2011 production dataset with *MTA* requires between 3,000 and 6,000 cpu-hours. In practice, to achieve fast turnaround, a subset of the full production data is analyzed. Only when the analysis approaches the ultimate precision is it necessary to include the full dataset to characterize the effects of analysis cuts.

Blinding MuSun implements a blinding scheme for the R2011 data, such that the analysis is performed with no advanced knowledge of the result. This ensures freedom from bias to agree with the results of theoretical calculations. Blinding is implemented by a detuning of the master clock frequency during experimental data taking. The nominal clock frequency is 500 MHz, but an associate of the collaboration secretly adjusted this to within the range 498.5 MHz to 499.5 MHz. However, because this same frequency was chosen for the $\mu+$ as well $\mu-$ data, it is still possible to extract the unblinded capture rate, Λ_d, at the precision afforded by the $\mu+$ statistics. A relative blinding between $\mu+$ and $\mu-$ datasets was implemented in the fitting software that extracts these rates, obscuring any possibility of extracting Λ_d, and allowing these two datasets to be unblinded separately. In addition, to encourage analysis teams at different institutions to analyze data with independent algorithms, a relative blinding between institutions has been implemented. Both of these software blindings require that a specific package of software be used to fit any high-statistics decay time distribution. The analytical power of blinded algorithms proved to be very useful in the MuLAN and MuCap experiments, so MuSun intends to maintain this strategy.

3.1.2 Electron tracking

The muon decay electrons are detected with a cylindrical hodoscope consisting of a double layer of scintillator paddles for good timing resolution and two multi-wire proportional chambers for tracking. The goal of the electron analysis is to identify these decay events and associate them with muon stops in the fiducial volume of the TPC. This association is achieved by constructing electron tracks from the information provided by the two multi-wire proportional chambers and the scintillators. Each reconstructed electron track is labeled with both a unique time, given by the scintillator photomultiplier tubes, and a vector that points back to the TPC. Cuts on the impact parameter between the muon stop position and the reconstructed electron track are then imposed to remove muon stops outside of the fiducial volume and the accepted tracks are then used to fill the final decay time histogram. At the same time, electron can be used for a tomography measurement of muon stopping locations. In this analysis, the z-coordinate of the muon stop is estimated by the point of closest approach between the electron track and the virtual beam axis (Fig. 23).

MuSun has inherited the bulk of the electron analysis from the MuCap experiment. This includes clustering algorithms for the wire chambers, electron track definitions and the general framework with which these elements are processed and associated with other detector systems. There is currently an effort to change parts of this inherited electron analysis framework. The goal is to create individual electron objects (eg. a cluster in the inner wire chamber) in the first stage of the analysis and leave the tracking reconstruction for the second stage. This is in contrast to the MuCap approach, in which the electron analysis was performed in the first stage and the electron track definition required, as a *seed* to generate the track, a four-fold coincidence in the four photomultiplier tubes reading out a double scintillator layer. The new electron analysis in the first stage is then solely comprised of algorithms that scan the individual electron detectors and form *seedless* electron objects out of them. These global electron objects are then associated with events in the muon entrance detectors and exported to the second analysis stage where multiple electron track definitions can be implemented with ease. This approach is more flexible and enables more freedom in exploring the impact of track reconstruction and muon-electron association on the final lifetime result.

3.1.3 Neutrons

Muons in pure deuterium produce two sources of neutrons: (i) fusion neutrons following $dd\mu$ molecule formation and the subsequent $dd\mu \rightarrow^3 He + n + \mu$ fusion reaction, and (ii) capture neutrons following the $\mu d \rightarrow n + n + \nu$ capture reaction. The $d\mu d$ fusion neutrons are monoenergetic with energy 2.45 MeV. The capture neutrons have a continuous energy spectrum that peaks at 1-3 MeV and extends to 53 MeV.

Encoded in the time dependence of the fusion neutrons are the two $dd\mu$ molecular formation rates from the $F = 1/2$, $3/2$ hyperfine states (λ_q and λ_d) and the hyperfine transition rate (λ_{qd}) from the higher-energy $F = 3/2$ state to the lower-energy $F = 1/2$ state. Knowledge of these parameters is important for the extraction of the μd doublet capture rate from the decay electron time distribution. In addition, the neutrons provide information about muon capture on materials other than deuterium, including gas impurities and wall materials.

All eight liquid-scintillator neutron detectors were calibrated with ^{60}Co and ^{137}Cs gamma source. Additionally, the two time-coincident gamma rays from ^{60}Co yield a relative timing calibration.

Neutron and γ-ray pulses can be distinguished on the basis of their pulse shapes. The neutron pulses have a longer tail compared to γ-ray pulses. A new method for n-γ discrimination was developed based on pulse templates. To generate the template, an average of pulses is formed in an energy regime where discrimination is easy. A template is generated for neutron and γ-ray pulses separately for each individual detector.

A computationally efficient single parameter fit of the template to a neutron-detector pulse was developed, using Brent's minimization method, fitting the pulse time t_j and then determining the pedestal and area normalization analytically. The difference in χ^2 between templates quantifies the n-γ discrimination (Fig. 21). Fig. 22 shows that a significant improvement was achieved over earlier methods.

In addition, the template-fit method allowed us to include overflow pulses, as the points beyond the FADC limit were ignored during the fit. The dynamic range used to be limited to 1630 keV$_{ee}$, using the slow-to-total n-γ discrimination method, and is now extended to nearly 2500 keV$_{ee}$[5].

---

[5]A 2.45 keV fussion signal leaves about 800 keV *equivalent electron* ee energy deposition in the neutron detector.
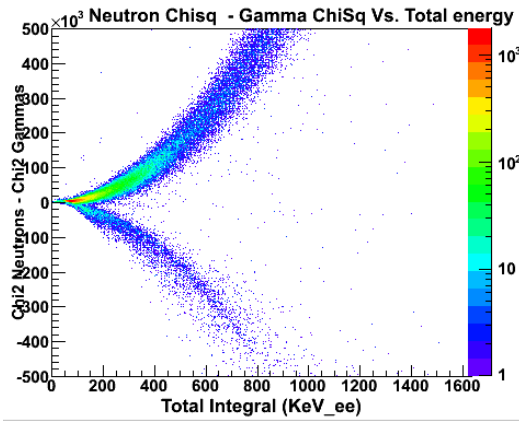
Figure 21: Difference between the chi squares of pulses first fitted with a neutron template and a gamma template versus energy for 'NU3' neutron detector
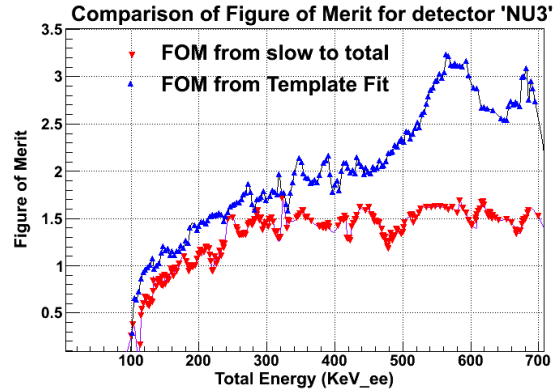
Figure 22: Figure of merit using tail to total integral analysis (in red) overlaid on template fit analysis (in blue). The figure of merit is defined as the separation of the neutron and γ band in Fig. 21 and Fig. 21 in [10], normalized on their FWHM.

3.1.4 TPC acceptance and muon losses

About 60% of the muons passing through the entrance detectors are stopped in the TPC, half of those in the fiducial volume[6],. The combination of electron track tomography (Fig. 23) GEANT4 simulations (see sect. 3.2) and the high-purity germanium X-ray detector (see Fig. 25 in [10]), form a powerful tool to explain the loss of 40% of muons seen by the entrance detectors.

About 50% of those muons still have a 2 μs lifetime and do not show up in the prompt X-ray spectrum, indicating that they stop in the D_2 gas outside the TPC. Electron tomography studies show that 3-5% of the muons stop in the steel field guiding wires at the entrance of the TPC. This is supported by 3-4% stops in steel as seen by the X-ray detector. In the future, thinner wires will be used. Fig. 23 also shows 2% of muons stop in the beryllium entrance window and its support structure[7].

Muon stops in the cathode are at the 2% level or less, and the 100 μm thick layer of silver stops all of those, shortening their lifetime to 88 ns. Less than 2.5% stop in the pad plane. However, the 5 μm thick Au layer on the anode pad was not sufficient to stop all muons. This issue is resolved by adding a 40 μm thick silver layer on the new pad plane (Sect. 2.3.3). Stops in the chamber walls or the TPC support structure are at the sub-percent level. About 5-10% of the muons remain unaccounted for.

The newly developed electron-tomography analysis module will provide a more detailed picture of the muon stop distribution and will improve our understanding of an impact parameter cut. Future hardware upgrade plans will depend on these results.

3.2 Monte-Carlo simulations

The MuSun Monte-Carlo package, based on GEANT4, has a detailed description of the apparatus, records hits in all sensitive detector volumes, and includes the atomic physics involved in μ^- capture on deuterium. Studies to date targeted specific questions such as where do the muons stop, how much do the Michel electrons interfere with muon tracking in the TPC, and

---

[6]Defined as the 24 central pads and a 15 mm cut from the top and bottom of the TPC.

[7]Note that the Monte-Carlo simulation estimates the entrance window and field wire stops about a factor of 2 larger.
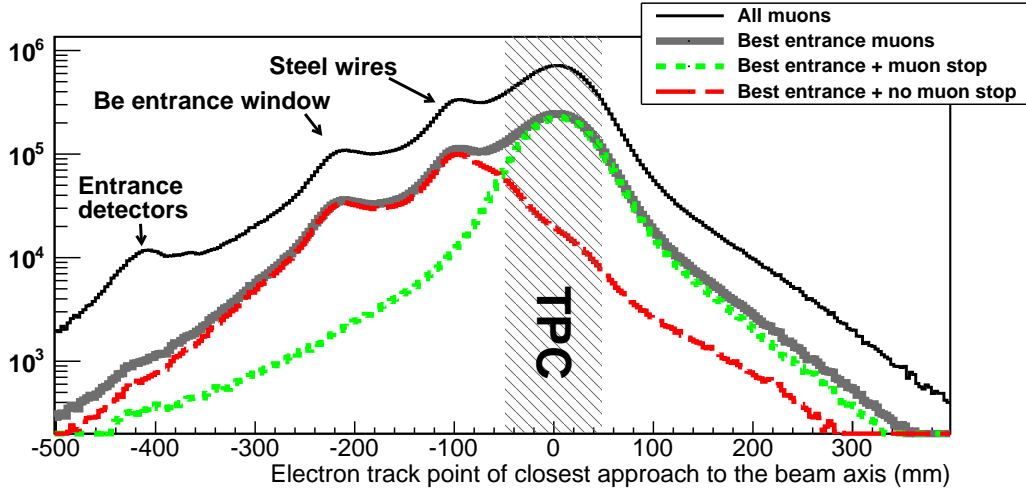
Figure 23: Electron tomography picture of the muon stops. The "Best Entrance" condition set by the entrance detectors cleans up the far upstream stops. Requiring a muon stop selects mostly tracks that point back to the TPC, cutting features such as tracks originating in the Be window. Most of the electron tracks with no associated muon stop point upstream. Note that the electron tracking resolution is smeared by scattering from the TPC pressure vessel, leading to long tails far from the TPC.

is it possible to use only the upstream pads in a muon stop definition, minimizing the effect fusion interference?

The entire Monte-Carlo chain consists of a GEANT4 simulation, a post-processing code folding in detector response and generating raw data files, which in turn are analyzed by our standard analysis software. Significant improvements over the last year will make it possible to create datasets of 10^8 events, allowing us to ask more general questions, such as the robustness of the muon stop definition.

3.2.1 Electronics response model

A second stage in the Monte-Carlo simulation reads the output of GEANT4, models the response of the detector and electronics, and produces a MIDAS file that can be interpreted by the analysis software in the same way as the raw data from the experiment. This program was enhanced substantially in Summer 2012 as an undergraduate research project at Regis University.

The pulse shapes generated for TPC signals had been entirely *ad hoc*, mostly generated by a Gaussian smearing of energy along a vertical axis. This model was replaced by a much more realistic one based on the operation of the electronics. A SPICE simulation of the amplifier chain (preamplifier, shaping amplifier, and baseline restorer) was tuned until it agreed with the measured electronic response. The pulse shape as it left the shaping amplifier was taken to be linear in the energy deposited. The baseline restorer was then modeled as a charging and discharging capacitor whose voltage is subtracted from the shaping amplifier output.

The model of the noise of TPC plus readout was also made much more realistic. A program was developed to calculate the noise power spectral density for blank waveforms that were collected in R2011. This spectrum was used to define the input parameters to the AbsRand library [11], which generates $1/f^\alpha$ correlated noise. The power spectral density of the generated noise was then verified to match that of the recorded noise.

A number of other features were added: the μPC was modeled for the first time, and

GEANT4 "truth" data is copied into the MIDAS file. The speed of the detector response program was improved dramatically, making it practical to use it to generate significant large datasets.
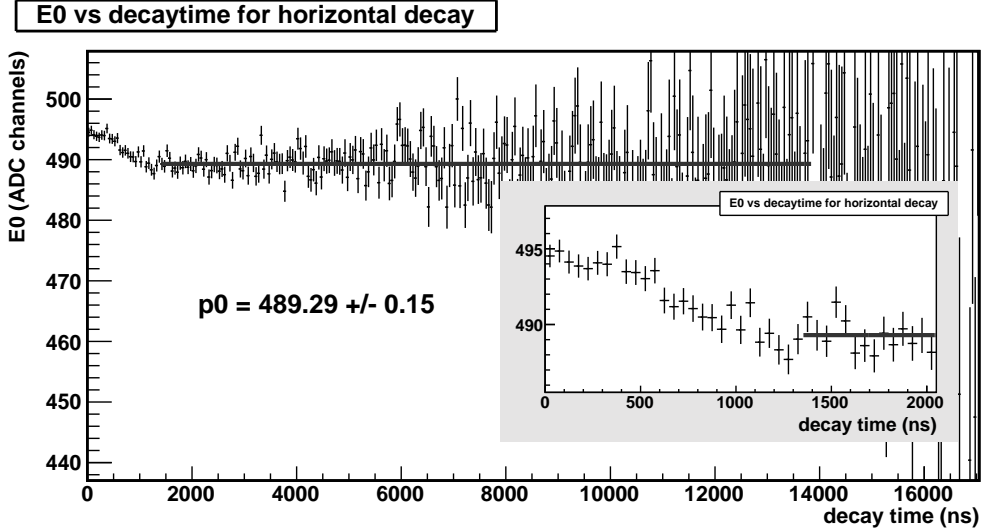
3.2.2 μ-e interference

Figure 24: The energy deposited in the Muon stop pad as a function of drift time using data from R2011.

Muon-electron interference occurs when Michel electrons ionize the deuterium gas and deposit energy on the TPC anode pads. Due to this, certain Michel electron signals from decays at early times overlap with the original muon pulse, changing the muon pulse fitting results and affecting the muon stop definition. This phenomenon can introduce a time-dependent acceptance, distorting the final lifetime fit and is therefore a potentially dangerous systematic effect. Our Monte-Carlo simulation is used to estimate this effect.

Typical Michel electron signals in the TPC are of the scale of a few percent compared to the muon signal, with a pulse shape highly dependent on the electron track direction and the initial vertex within the stop pad. After a full GEANT4 simulation, the post-processing stage generates two output files, one with and one without the electron interference, saving the electron track parameters in the truth bank. The files are then processed with our standard *MU* and *MTA* analysis packages. From this, we expect that the number of accepted muon stops from the μ^--only dataset compared to the μ^- with electron interference dataset to be slightly different. This method is still under development, but we are close to having a working tool.

A less accurate but faster approach to estimate the electron-interference effect is to fold Monte-Carlo generated electron pulses with the muon pulses from R2011 data. From this a look up table is generated containing information, such as energy, derived from the fit to the muon-electron pulse, as function of electron decay direction and time. Preliminarily, selecting only events with horizontal electron tracks, we estimate that about 0.04% of muon pulses on the stop pad are boosted above a 100 keV energy threshold.

At the same time, electron interference was observed in the R2011 data. From the simulation, we know that early (<1 μs) decay electrons with a horizontal trajectory in the TPC produce a larger interference effect than electrons moving in the vertical direction. After a cut

22

for horizontal electron tracks, the mean energy deposition in the stop pad, E_0, changes by 1% for early versus late (>1 μs) decays (Fig. 24). Currently, we are working reproducing these results with simulations. With a better energy calibration and further simulation software development, we are confident that we will reach good agreement.

3.2.3   Upstream pads stop definition

The interference of $dd\mu^-$ fusions with the muon stop identification via modification of the energy deposition near the stopping point is of great concern. In particular, the proton from $dd\mu^- \to \mu^- tp$ has a range of 16 mm, so it can leave the fiducial volume, rejecting the event in a time-dependent way, thus affecting the lifetime measurement.

If our energy resolution is good enough, and the μ^- energy deposition doesn't fluctuate too much, we can use the upstream pads to determine the μ^- stopping point without bias from fusion products.

To investigate this we have parameterized the GEANT4 muon energy deposition as a function of distance from the stopping point. Because the muon energy loss per mm increases near the end of the track, the integral over the pad gives us a measure of distance to the stop point. We fit all pads excluding the two most downstream to the expected muon energy deposition to determine the stopping point. For Monte Carlo events we can directly check how accurate the result is. We can also use only the last two pads which allows a direct comparison with μ^+ data, where there are no fusions and the energy deposition in last two pads yield an accurate estimate of the muon stop position.

Convoluting the Monte Carlo energy deposition with a 40 keV resolution and introducing a 150 keV threshold gives a reasonable agreement with data as shown in Fig. 25. The long tail to the right, where the upstream pads predict the muon stops further downstream than it really does, are due to muons clipping the corner of a pad so the ionization collected by the pad is below threshold and is lost. We would incorrectly reject some of these events as possibly leaving the TPC but that just affects efficiency and does not introduce a bias. Decreasing the threshold decreases the tail on this side. The tail to the left is more of a concern since it may include events where we think the muon stayed in the TPC but in fact it did not. Improving the energy resolution makes the distribution narrower on this side. These results are encouraging but we need to check them with a realistic detector simulation and larger statistics.

3.2.4   Large Monte Carlo Event Samples

With the entire simulation chain complete, from GEANT4 event generation through detector response and then the standard data analysis, we want to generating large samples of events for general purpose studies. The current GEANT4 simulation package takes about one hour on one core to simulate 10^6 μ^+ events, producing an output file of 2.3GB. It takes 70 minutes to process this file through the detector response, producing another similarly sized file, and then about 15 minutes through a standard analysis. Scaling to 10^8 events we expect it will take ten cores just over a day, producing files taking up about 500 GB of storage.

Before proceeding to a Monte Carlo sample of this size we plan to validate the simulation chain on samples of a few 10^6 events. We have indications some of the support structure may need to be modified, we need to check that the electronics response matches the electronics in the experiment, and we need to complete debugging the atomic physics descriptions of the μ^- capture.
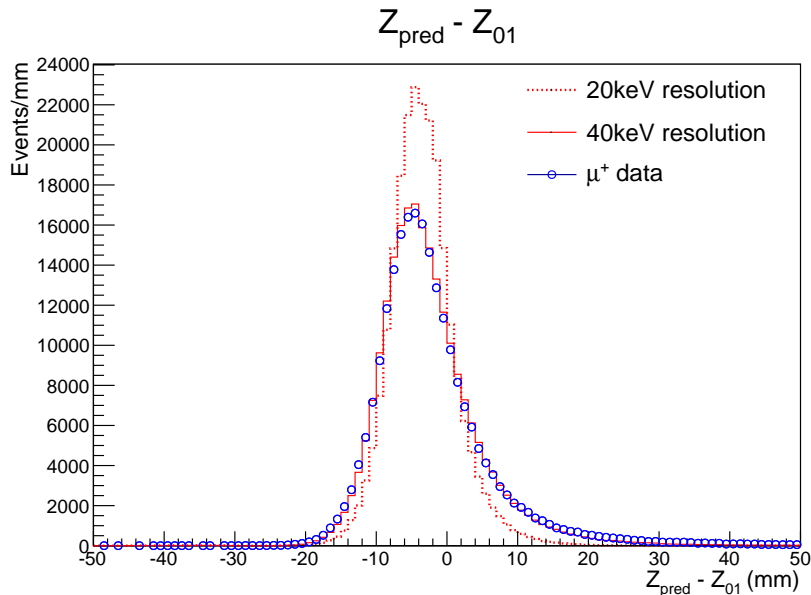
Figure 25: Comparison of stopping position determined from upstream pads with position determined by last two pads. Z_{pred} is the stopping point determined by fitting the upstream pad energy deposition, excluding the last two pads. Z_{01} is the stopping point determined by fitting the last two pads and is much more accurate than Z_{pred}. The blue points are μ^+ data. The red lines are Monte Carlo simulation, the solid line has a 40 keV energy resolution and 150 keV threshold while the dashed line has a 20 keV energy resolution and 60 keV threshold.

4 Plans and Beam Time Request 2013

4.1 Upgrade Plans

4.1.1 Beamline

For the requested Fall 2013 run, two new quadrupole triplets will be ready as well as a remotely controlled non-magnetic slit system inside the bending magnet ASK51. The increased acceptance and the more flexible beam collimation should allow to keep the electron suppression and kicker muon extinction at the 2012 values, while increasing the incident muon beam rate and stopping fraction. In addition, the transverse positioning system of the TPC will be improved so that it can be more easily adjusted for optimal muon stopping conditions.

4.1.2 TPC Resolution

Excellent TPC energy resolution is necessary in many respects, but it is critical for two measurements in particular: a determination of the muon stop location in a manner robust against fusion interference and an *in-situ* detection of nuclear recoils resulting from muon capture on impurities underneath the background of the ubiquitous ^{3}He fusion signals.

As the TPC has no gas gain and the generated signals are small (4.4 fC/MeV), there are potentially several important noise sources affecting the resolution, including i) intrinsic preamplifier noise, ii) rf pickup and iii) acoustics induced by the cold head compressor. Our tests with the new cryo-preamplifiers during R2012 demonstrated remarkable improvements regarding sources i) and ii), as discussed in section 2.3.2. Thus we plan to implement a full cryo-preamp readout system. The development path includes:
- further optimization of circuit resolution, power consumption and prototyping,

- design miniature 8-channel preamp/driver card for cryogenic operation,
- extensive tests in the TPC setup at UW, including testing at LN2 temperature,
- design of a dedicated LN2 cooling loop for the new preamps in the TPC vacuum enclosure,
- installation and commissioning at PSI June-July 2013.

We will further study the sources of the acoustics, in particular the TPC support and the effect of coaxial high vacuum cables inside the TPC vessel, replacing the flexible Kapton cables used presently. On the electronic side, we will increase the filtering at the preamp stage, and continue to employ a baseline restorer at the final amplifier, which worked very well. In addition, we will explore digital filtering techniques with the TPC ADCs.
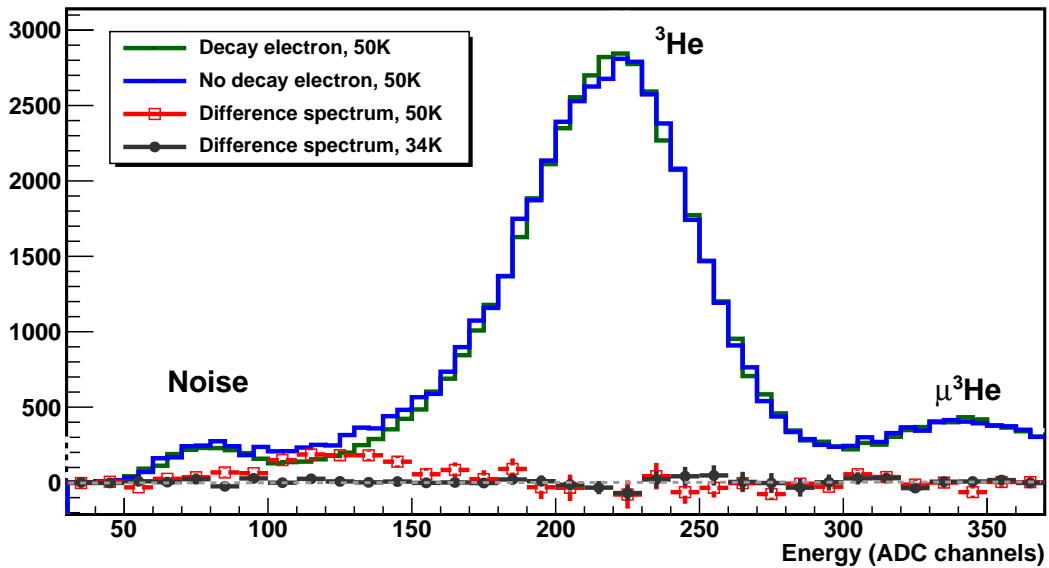
4.1.3 Gas Purity

Figure 26: An excess of counts were observed in the delayed TPC spectrum between 100 keV and 200 keV for events with no decay electron versus events with an electron hit, i.e. events with no muon capture(R2011 data). Nuclear recoil signals from muon capture on gas impurity are expected in this energy range (see Fig. 11 in [?]). The number of counts follows the same trend as the observed signal losses versus drift time (Fig. 28 in [10]), disappearing within error bars at 34 K. Due to the high background from the ^{3}He it is hard to make a quantitative statement about the impurity concentration, however, we aim to an improved sensitivity with the ongoing preampifier and X-ray detector developments.

As detailed in our our original proposal [9] and more recently in our 2011 progress report [10], the MuSun experiment requires ultra-high purity deuterium gas at the 1 ppb level. An important step towards this goal was the refurbishment of our continuous purification system CHUPS during 2012, which recovered its design flux of 3 L/min with fresh, cleaned filters. We also hoped to cool from 34 K to lower temperatures. Several small heat leaks were fixed, but while the cooling capacity increased, we did not reach the anticipated 30 K. Currently the cold head is being serviced, which might solve this issue.

The most difficult problem, however, is the verification and monitoring of the purity at the required level. We investigate two monitoring methods: i) Measuring of impurity capture

yield within TPC(Fig. 26), ii) gas analysis of the exit flow from the TPC.

As demonstrated by MuCap, i) is the preferred method as the impurities are measured in-situ and the correction on the lifetime can be directly related to the impurity concentration, by controlled doping of the TPC gas with higher impurity levels. We will analyze our sensitivity based on the improved TPC resolution attained with the cryo-preamplifiers in R2012. We will also use the 2012 X-ray data (Sect. 2.3.4) to decide whether we should build an X-ray tagging NaI array.

As regards the gas analysis method ii), a stainless steel line was installed in 2012, so that the sampling gas stream bypassed the TPC exit heat exchanger, where additional surface reactions might occur. In spite of these improvements, we have not demonstrated that 1 ppb sensitivity can be reliably achieved with our gas chromatography system (GCS). A measuring program is being prepared at PNPI using N_2+D_2 gas mixtures in the temperature range 20-50K. By following the vapor pressure curve, the sensitivity, reproducibility. and calibration of the GCS will be established. If the results are insufficient, we will develop a impurity concentration system (ICS). By inserting a getter into the circulation system, the sensitivity can be dramatically increased compared to the present method of analyzing limited gas volumes extracted from the CHUPS circuit. All methods need careful calibrations with doped gas quantities of known concentrations.

4.1.4 Additional Upgrades

While the pad plane manufacturing with thick silver plating has been successful, the grid field was limited to about 24 kV/cm, before sparking was observed. New frames with Frisch grids will be built to increase the HV compatibility. Sparking, which might damage the cryo-preamplifier FETs, has to be avoided, as their replacement is complicated by their planned location inside the isolation vacuum. Tests of the system will be performed at the UW TPC set-up.

The ancient LeCroy HV system for the 64 electron detector scintillators died during R2012, and is being replaced by a newer CAEN system. The hardware has already been exchanged, software control and feedback still have to be implemented.

4.2 Beam Request

In 2013 we request beam time for a first full MuSun production run in πE1, with the following planned schedule.

- 2 weeks: Commissioning the final beam at the experiment, integrating the new beam elements described above. Set-up of the experiment for production with beam.

- 8 weeks: Production to collect a statistics of 1×10^{10} $\mu-e$ events, 70 % μ^- and 30 % μ^+. Here events refers to fully reconstructed pairs, which pass all final analysis cuts.

- 2 weeks: Measurement program will be directed towards the demanding purity issue. This will include temperature cycling and doping the gas with enhanced concentrations of nitrogen and oxygen.

For this program, we need and request three full 4 week periods of πE1 beamtime.
The start of the beam period must be after August, compatible with the commissioning of the new quadrupole triplets and the time required to perform the planned upgrades to the experiment. In order to facilitate the participation of teaching faculty, a start date of Sept. 2, 2013 would be ideal, while Sept. 30, 2013 would be also acceptable.

References

[1] MuSun Collaboration (http://muon.npl.washington.edu/exp/MuSun):
V.A. Andreev, E.J. Barnes, R.M. Carey, V.A. Ganzha, A. Gardestig, T. Gorringe, F.E. Gray, D.W. Hertzog, M. Hildebrandt, L. Ibanez, P. Kammel, B. Kiburg, S.A. Kizilgul, S. Knaack, P.A. Kravtsov, A.G. Krivshich, K. Kubodera, B. Lauss, M. Levchenko, X. Luo, K.R. Lynch, E.M. Maev, O.E. Maev, F. Mulhauser, M.H. Murray, F. Myhrer, K. Neely, A. Nadtochy, C. Petitjean, G.E. Petrov, J. Phillips, R. Prieels, D. Prindle, N. Raha, R. Ryan, G.N. Schapkin, N. Schroeder, G.G. Semenchuk, M.A. Soroka, V. Tishchenko, A.A. Vasilyev, A.A. Vorobyov, N. Voropaev, M.E. Vznuzdaev, F. Wauters, P. Winter.

[2] Kammel, P. and Kubodera, K. *Annu. Rev. Nucl. Part. Sci.* **60**, 32753 (2010).

[3] Marcucci, L., Kievsky, A., Rosati, S., Schiavilla, R., and Viviani, M. *Phys.Rev.Lett.* **108**, 052502 (2012).

[4] Adam, J., J., Tater, M., Truhlik, E., Epelbaum, E., Machleidt, R., et al. *Phys. Lett. B* **709**, 93–100 (2012).

[5] Bardin, G. et al. *Nucl. Phys. A* **453**, 591 (1986).

[6] Cargnelli, M. et al. In *Proceedings of the XXIII Yamada Conf. on Nuclear Weak Processes and Nuclear Structure, Osaka, Japan*, (1989).

[7] Chen, J.-W., Inoue, T., Ji, X.-d., and Li, Y.-C. *Phys. Rev. C* **72**, 061001 (2005).

[8] Andreev, V. et al. (2012). arXiv:1210.6545.

[9] Andreev, V. et al. (2010). arXiv:1004.1754.

[10] MuSun Collaboration. (2011). Progress Report 2011 and Beam Request for 2012.

[11] Plaszczynski, S. *Fluctuation and Noise Letters* **7**, R1–R13 (2007). http://planck.lal.in2p3.fr/wiki/pmwiki.php/Softs/AbsRand.